Plasma environment of Mars as observed by simultaneous MEX-ASPERA-3 and MEX-MARSIS observations

E. Dubinin,[1] R. Modolo,[2] M. Fraenz,[1] J. Woch,[1] G. Chanteur,[3] F. Duru,[2] F. Akalin,[2] D. Gurnett,[2] R. Lundin,[4] S. Barabash,[4] J. D. Winningham,[5] R. Frahm,[5] J. J. Plaut,[6] and G. Picardi[7]

[1]   Simultaneous in situ measurements carried out by the Analyzer of Space Plasma and Energetic Atoms (ASPERA-3) and Mars Advanced Radar for Subsurface and Ionospheric Sounding (MARSIS) instruments on board the Mars Express (MEX) spacecraft for the first time provide us with the local parameters of cold ionospheric and hot solar wind plasma components in the different regions of the Martian magnetosphere and ionosphere. On the dayside, plasma of ionospheric and exospheric origin expands to large altitudes and gets in touch with the solar wind plasma. Formation of the magnetic field barrier which terminates the solar wind flow is governed by solar wind. The magnetic field rises up to the value which is just sufficient to balance the solar wind pressure while the position of the magnetospheric boundary varies insignificantly. Although, within the magnetic barrier, solar wind plasma is depleted, the total electron density increases owing to the enhanced contribution of planetary plasma. In some cases, a load caused by a planetary plasma becomes so strong that a pileup of the magnetic field occurs in a manner which forms a discontinuity (the magnetic pileup boundary). Generally, the structure of the magnetospheric boundary on the dayside varies considerably, and this variability is probably controlled by the magnetic field orientation. Inside the magnetospheric boundary, the electron density continues to increase and forms the photoelectron boundary which sometimes almost coincides with the magnetospheric boundary. The magnetic field strength also increases in this region, implying that the planetary plasma driven into the bulk motion transports the magnetic field inward. A cold and denser ionospheric plasma at lower altitudes reveals a tailward cometary-like expansion. Large-amplitude oscillations in the number density of the ionospheric plasma are another typical feature. Crossings of plasma sheet at low altitudes in the terminator region are characterized by depletions in the density of the ionospheric component. In some cases, density depletions correlate with large vertical components of the crustal magnetic field. Such anticorrelation in the variations of the densities of the cold ionospheric and hot magnetosheath/plasma sheet plasmas is also rather typical for localized aurora-type events on the nightside.

1.   Introduction

[2]   Although space missions to Mars prior to Mars Global Surveyor (MGS) and Mars Express (MEX) have established the existence of the main plasma domains [see, e.g., *Nagy et al.*, 2004], the low-altitude region ($h \leq$ 800 km), in which the magnetospheric obstacle is forming and processes of solar wind induced escape of the planetary atmospheric/ionospheric matter are expected to be most efficient, was not explored. The MGS measurements have shown that, at present, Mars does not possess a global intrinsic magnetic field which could be an obstacle for solar wind [*Acuña et al.*, 1998]. Instead, MGS has detected localized, rather strong magnetic anomalies of a crustal origin. Owing to the absence of a magnetic obstacle at Mars the solar wind directly interacts with its upper atmo-

[1]Max-Planck-Institute for Solar System Research, Katlenburg-Lindau, Germany.
[2]Department of Physics and Astronomy, Iowa University, Iowa City, Iowa, USA.
[3]Centre d'Etude des Environnements Terrestres et Planétaires, IPSL, Velizy, France.
[4]Swedish Institute of Space Physics, Kiruna, Sweden.
[5]Southwest Research Institute, San Antonio, Texas, USA.
[6]Jet Propulsion Laboratory, Pasadena, California, USA.
[7]Infocom Department, "La Sapienza," University of Rome, Rome, Italy.

sphere and ionosphere, and induces a magnetosphere by the pileup of the interplanetary magnetic field. A similar type of interaction occurs around another nonmagnetized planet, Venus, and was extensively explored by the Pioneer-Venus-Orbiter (PVO) during 14 years of operation [see, e.g., *Russell et al.*, 2006]. Although the PVO mission has provided a wealth of excellent in situ data about the solar wind/ionosphere interaction for a wide range of solar wind conditions, the plasma ion component in the energy range ~10 eV to 10 keV was studied rather poorly because of instrument and telemetry constraints. Since MGS was also not equipped with a plasma instrument for the measurement of ion components, only the MEX mission could partly fill this gap.

[3] The measurements made by the ASPERA-3 experiment on board MEX have shown that a magnetospheric cavity almost void of the solar wind plasma is formed at Mars [*Dubinin et al.*, 2006b]. The median positions of the magnetospheric boundary in the subsolar and terminator region are ~650 and ~1350 km, respectively. Crustal magnetic fields create an additional protection from solar wind plasma on the dayside of the southern hemisphere [*Fraenz et al.*, 2006; *Dubinin et al.*, 2008a]. Since the thermal ionospheric pressure is unable to balance the incident solar wind pressure at such distances [*Hanson et al.*, 1977], the real obstacle for solar wind could only be the induced magnetic field. The evidence of the formation of a magnetic barrier at Mars was the observation of the magnetic pileup boundary (MPB), a sharp boundary with a strong jump in the magnetic field strength, a drop in the magnetic field fluctuations, and a strong decrease in the superthermal electron fluxes [*Acuña et al.*, 1998]. However, the questions of whether and how the solar wind gets in a touch with the Martian ionosphere, which is the necessary condition for the generation of induced currents, remained open because of the absence of measurements of the cold plasma component. An important advance came from the MARSIS active radar experiment on MEX which could provide the local plasma parameters (electron density and magnetic field strength) by measuring the plasma wave echoes excited by the radar transmitter [*Gurnett et al.*, 2005].

[4] The Martian ionosphere, formed by the photoionization of the major neutral constituents CO_2 and O with subsequent molecular reactions creating O_2^+ as the major ionospheric ion species and O^+ becoming comparable at altitudes ≥ 300 km was poorly explored as compared to Venus. The measurements of the main ionospheric characteristics at Mars were made in situ by the two Viking landers [*Hanson et al.*, 1977; *Hanson and Mantas*, 1988], that provided us with two ionospheric height profiles, and by radio occultation experiments [*Kliore*, 1992]. Recently new radio occultation measurements were carried out on board the MEX spacecraft [*Pätzold et al.*, 2005]. Most of the radio occultation profiles show a relatively extended ionosphere without clear ionopause structure. A radar sounding technique used on the MEX spacecraft is able to get vertical profiles of the electron density in a broad range of solar zenith angles (SZA) and with much higher horizontal spatial resolution as compared to the radio occultation experiments which measure column densities integrated

along the line of sight [*Gurnett et al.*, 2005, 2007; *Duru et al.*, 2008].

[5] The ionospheric plasma was also traced on MEX by the characteristic ''spectral lines'' of photoelectrons which were resolved owing to the high energy resolution of the electron spectrometer in the ASPERA-3 plasma package [*Frahm et al.*, 2006a]. The ionospheric electrons were measured in a wide range of altitudes and the boundary of the photoelectrons (PEB) was observed rather far from the planet and close to the magnetospheric boundary even near the terminator and further in the tail [*Dubinin et al.*, 2006b; *Frahm et al.*, 2006b]. However, it has remained unclear as to whether the PEB and the ionopause are collocated since the cold ionospheric component and their contribution to pressure could not be measured by the ASPERA sensor.

[6] The MARSIS sounding experiment on MEX is able to trace not only ionospheric height profiles below the spacecraft but also to provide us with the local plasma number densities from locally excited electron plasma oscillations [*Gurnett et al.*, 2005, 2007; *Duru et al.*, 2008]. Whereas the density measurements from the remote sounding measurements are generally confined to the altitudes 130 – 300 km, the electron plasma oscillations give the local number densities in the altitude range from 275 to 1300 km. *Duru et al.* [2008] have compared the results from the two techniques in the SZA range between 30° and 60° and shown that, at the altitudes below ~200 km, where the photochemistry dominates, the Chapman photo-chemical equilibrium model is a good approximation to the density profile [see also *Gurnett et al.*, 2005, 2007; *Morgan et al.*, 2008]. At higher altitudes, where upward diffusion and horizontal plasma transport becomes important, the ionospheric characteristic height scale increases. Moreover, the Martian ionosphere, above 300 km, becomes very dynamic and is strongly influenced by the solar wind. The recent upgrade of the ion mass spectrometer, which is a part of the ASPERA-3 experiment, carried out the first measurements of the cold/low-energy ions in this region. *Lundin et al.* [2008] have observed a mantle of low-energy ionospheric ions swept from the dayside over the terminator, expanding into the tail in a ''comet-like'' fashion. It is suggested that this ion component is a major source of ion escape from Mars.

[7] Recently, simultaneous measurements of the local plasma parameters of the ionospheric and solar wind plasmas, and the magnetic field strength were performed by the ASPERA-3 and MARSIS experiments in the subsolar region of the induced Martian magnetosphere. For the first time the pressure balance across the solar wind/ionosphere interface was evaluated [*Dubinin et al.*, 2008b]. It was shown that in a broad range of the solar wind dynamic pressures, the magnetic field in the boundary layer raises to the values just sufficient to balance the solar wind pressure. Here we continue the comparative study of plasma environment on Mars based on the simultaneous observations by the ASPERA-3 and MARSIS experiments on board the MEX spacecraft. In situ plasma and magnetic field measurements conducted by these instruments complement each other and for the first time provide us with the local parameters of cold ionospheric and hot solar wind components in the different regions of the Martian magnetosphere and ionosphere. We present the combined observations
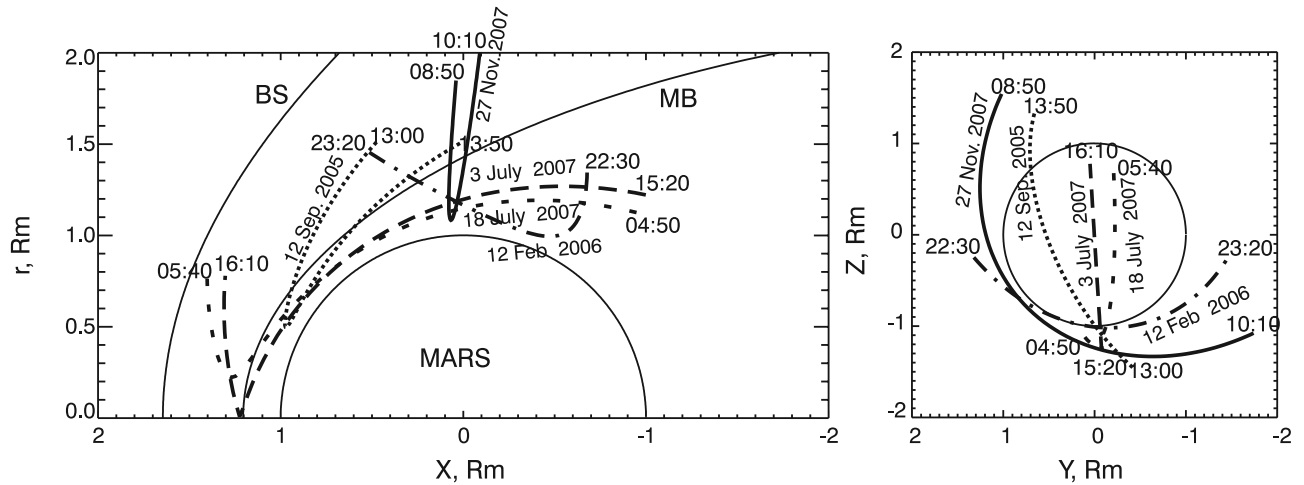
Figure 1. MEX orbits in MSO reference frame ($X_{MSO}-r$ and $Y_{MSO}-Z_{MSO}$ projections).

carried out on the dayside, near the terminator, and on the nightside to infer typical features of the plasma environment of Mars.

2. Instrumentation

[8] The MEX spacecraft is in a highly eccentric polar orbit around Mars with periapsis and apoapsis of about 275 and 10000 km, respectively. Figure 1 shows several typical MEX orbits (12 September 2005, 1300–1350 UT; 12 February 2006, 2230–2320 UT; 3 July 2007, 1520–1610 UT; 18 July 2007, 0450–0540 UT; 27 November 2007, 0850–1010 UT) the data from which are discussed in this paper. The left panel presents the orbits plotted in cylindrical X_{MSO}, $r = (Y^2_{MSO} + Z^2_{MSO})^{1/2}$ coordinates. The right panel depicts the $Y_{MSO}Z_{MSO}$ orbital projections. The used MSO reference frame has Cartesian components as follows: X_{MSO}, toward the Sun; Y_{MSO}, opposite to the planet velocity vector; Z_{MSO}, completes the right-hand system. The ASPERA-3 (Analyzer of Space Plasma and Energetic Atoms) experiment is a combination of in situ and remote diagnostics of atmospheric escape induced by the solar wind. It comprises the Ion Mass Analyzer (IMA), ELectron Spectrometer (ELS), Neutral Particle Imager (NPI) and Neutral Particle Detector (NPD) [*Barabash et al.*, 2006]. The Ion Mass Analyzer (IMA) determines the composition, energy, and angular distribution of ions in the energy range ≈10 eV to 30 keV. Mass (m/q) resolution is provided by combination of the electrostatic analyzer with deflection of ions in a cylindrical magnetic field set up by permanent magnets. A new configuration uploaded in May 2007 has further improved the IMA performance, improving the energy resolution of the cold/low-energy ions (≤50 eV). In the energy range ≥50 eV, IMA measures fluxes of different (m/q) ion species with a time resolution of ~3 min and a field of view of 90° × 360° (electrostatic steering provides an elevation coverage of ±45°). The measurements of the cold/low-energy component (≤50 eV) are carried out without the elevation coverage, and therefore, the time-resolution of these measurements increases up to 16 s. The ELS sensor measures 2D distributions of the electron fluxes in the energy range 1 eV–20 keV ($\delta E/E$ = 8%) with a field of view of 4° × 360° and a time resolution of ~4 s. The grid usually biased at −5V protects the sensor from the low-energy photoelectrons.

[9] The MARSIS (Mars Advanced Radar for Subsurface and Ionospheric Sounding) radar sounder ($f \approx 0.1$ to 5.5 MHz) on Mars Express is designed to monitor the ionospheric height profile and the subsurface of the planet [*Picardi et al.*, 2004]. It consists of a 40 m tip-to-tip electric dipole antenna, a radio transmitter, a receiver, and a digital signal processing system. For the normal ionospheric sounding mode used by MARSIS the transmitter steps through 160 frequencies ($\Delta f/f \approx 2\%$) from 100 kHz to 5.5 MHz. The receiver has a bandwidth of 10.9 kHz centered on the frequency of the transmitted pulse. A complete scan through all 160 frequencies takes 1.26 s, and the basic sweep cycle is repeated once every 7.54 s. The measurements were made in the region around periapsis, at the altitudes ≤1300 km. In addition to remote radio sounding, the local electron density and the magnetic field strength can also be obtained from MARSIS by measuring the frequencies of local electron plasma oscillations ($f_{pe} = (n_e e^2/\pi m_e)^{1/2}$) and their harmonics, and electron cyclotron waves ($f_{ce} = eB/2\pi m_e c$), excited by the radar transmitter in the nearby plasma [*Gurnett et al.*, 2005, 2007; *Duru et al.*, 2008]. If the plasma frequency is below the lower limit of the frequency of the receiver (100 kHz) which often happens at high altitudes, the electron plasma frequency cannot be observed. However, its harmonics generated by distortion in the preamplifier due to very large amplitudes of the waves still allow a determination of electron densities as low as 20 cm^{-3} by measuring the spacing of the harmonics. The accuracy for measuring the electron density is about of ±2% [*Gurnett et al.*, 2005, 2007; *Duru et al.*, 2008]. Some other factors (the harmonic spacing must be ≥30 kHz, plasma speed ≤160 km/s, the electron temperature ≤~0.73 n_e(cm^{-3}) eV) impose additional constraints on the density measurements ($n_e \geq 10–20$ cm^{-3}) [*Duru et al.*, 2008]. The electron cyclotron echoes, which are usually present in the magnetic fields greater than few tens of nT,
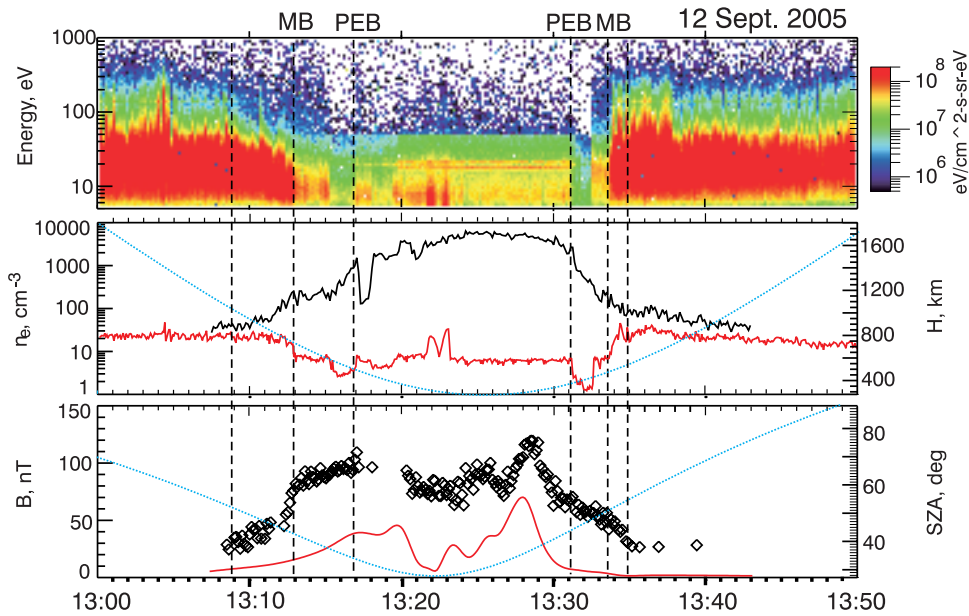
Figure 2. Observations made on 12 September 2005. (top) Spectrogram of electron fluxes. (middle) Electron number density of the hot component ($E_e > 5$ eV) measured by ASPERA-3 (red curve) and total number density from MARSIS (black curve). The blue curve shows the s/c altitude (right axis). (bottom) The magnetic field value from MARSIS (diamonds) and the crustal field model (red curve). Blue line, the solar zenith angle (right axis). Approximate locations of the magnetosphere boundary (MB) and photoelectron boundary (PEB) are marked with vertical dashed lines.

are excited by the cyclotron motion of the electrons accelerated by the radar wave pulses [*Gurnett et al.*, 2005].

3. Observations

3.1. Subsolar Region: Magnetic Field Barrier

[10] Figure 2 presents the observations made by ASPERA-3 and MARSIS on MEX from 12 September 2005 when the spacecraft crossed subsequently the dayside magnetosheath and magnetosphere. The top panel shows the energy-time spectrogram of the electrons. The drop of electron fluxes at 1313 UT corresponds to the entry into the magnetospheric cavity. At 1317 UT when the s/c was at ~500 km from the planet two narrow peaks in the range between 20 and 30 eV appear on the electron energy spectra. Their origin is associated with absorption of the strong HeII line at 30.4 nm in the carbon dioxide dominated atmosphere on Mars [see, e.g., *Frahm et al.*, 2006a]. A sudden drop of CO_2 photoelectrons was observed at 1331 UT ($H \sim 400$ km) on the outbound leg of the orbit. At 1333:30 UT MEX leaves the magnetosphere. Ionospheric photoelectrons with their characteristic peaks in energy spectra were often observed close to the magnetospheric boundary implying an important role of the ionospheric component in the formation of the induced magnetosphere [*Dubinin et al.*, 2006b]. However, the structure of the interface between the ionosphere and magnetosheath remained unclear. The middle panel depicts the electron number density by ASPERA-3 (the red curve shows the density derived from the moment calculations of the measured electron fluxes) and MARSIS (the black curve), respectively. MARSIS was able to measure the electron number density not only in the ionosphere but also in a dense magnetosheath plasma providing a rather

reasonable fitting with the ASPERA-3 measurements of a hotter ($E_e > 5$ eV) electron component of solar wind origin. Both curves begin to diverge closer to Mars indicating a progressive dropout of the solar wind and a dominance of a cold ionospheric component inside the magnetosphere. The important feature is the existence of a dense ($n_e \geq 100$ cm^{-3}) planetary plasma in the interface region. The absence of the characteristic CO_2 peaks on the electron spectra probably imply a change of ion composition. At the boundary of the photoelectron fluxes (PEB) the plasma density reaches values of more than 10^3 cm^{-3}. The bottom panel gives the magnetic field strength inferred from the MARSIS echoes (diamond symbols) and the value of the internal crustal field from the model by *Cain et al.* [2003] (the red curves). On the inbound leg, the inner magnetosheath (1309–1313 UT) is characterized by a gradual increase in the magnetic field value and the total electron number density, and also by a softening of the electron spectra. The onset of the field pileup is tentatively marked with the vertical dashed line. The inbound crossing of the magnetosphere boundary (MB) is characterized by an abrupt jump of the magnetic field. Such a transition corresponds to the magnetic pileup boundary (MPB) observed earlier not only on Mars, but also near other nonmagnetized celestial bodies as Venus and comets [*Acuña et al.*, 1998; *Mazelle et al.*, 1989; *Bertucci et al.*, 2003, 2005]. However, till now simultaneous plasma and magnetic field measurements were absent. The MARSIS data for the first time show that a crossing of the MPB occurs with an increase in the plasma density. The outbound MB is also characterized by an increase in the magnetic field value. An enhancement in the magnetic field strength also goes on in the region between the sheath and the ionosphere on both orbit legs.
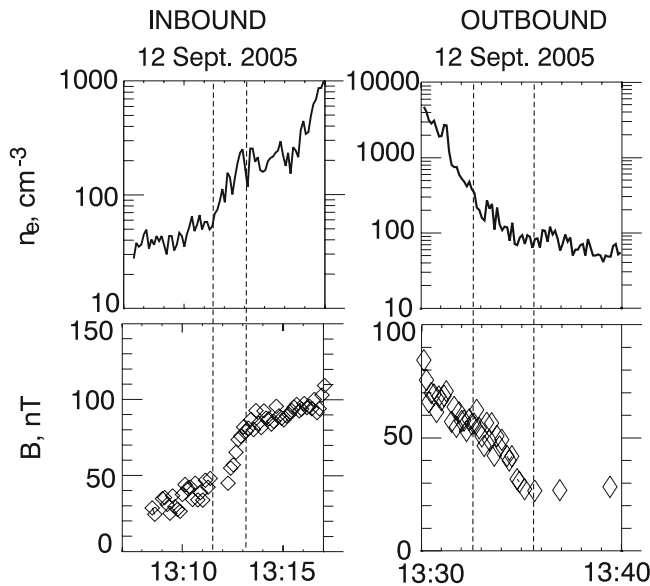
Figure 3. Variations in the electron number density and the magnetic field value across the inbound and outbound magnetospheric boundary. Vertical lines bound these transitions.

The peak in the field value recorded in the ionosphere at 1328:30 UT is likely associated with the compression of the crustal field. Figure 3 shows in more detail variations in the plasma density and the magnetic field across the MB on the inbound and outbound legs. The electron number density rises up to $\sim$200 cm^{-3}.

[11] Figure 4 presents another example of the MPB crossing on 9 July 2007 [see also *Dubinin et al.*, 2008b]. The magnetic field value reaches almost 100 nT. The boundary width of a sharp transition in the assumption of a static boundary is $\sim$30 km. The right panel shows several

subsequent energy spectra of ions. Solar wind and planetary ions are identified from the composition measurements and for convenience are marked by black and red, respectively. It is observed that there is a predominance of planetary (oxygen) ions at 1254 UT inside the magnetosphere and the prevalence of solar wind ions outside the magnetosphere (1304 UT and 1310 UT). The MPB crossing is characterized by a mixture of both ion populations (1301:05 UT).

[12] Another type of the solar wind/ionosphere interface is described by a gradual pileup of the magnetic field in the inner part of the magnetosheath. Such a magnetic barrier acts as an obstacle to solar wind at which the magnetic field pressure balances the ram solar wind pressure [*Dubinin et al.*, 2008b]. A feature of a gradual cooling of the sheath electrons accompanied by a pileup of the magnetic field with approaching the MB is rather typical and is observed at different solar zenith angles. Figure 5 presents the data obtained at small angles (SZA $\approx$ 0–40°) in the subsolar region. Although the spacecraft slew from the nadir to the communication orientation on the orbit on 3 July 2007 could affect the ASPERA-3 measurements, similar features are seen on other orbits. A diversity of the curves of the plasma density n_e measured by ASPERA-3 and MARSIS which is observed on all orbits imply a gradual decrease (increase) in the density of solar wind (planetary) plasma. These features indicate a mass loading of the shocked solar wind with planetary ions accompanied by ionization losses of the high-energy component of solar wind electrons. The loss of solar wind protons can also be due to charge exchange processes and squeezing along the draped field lines.

[13] It is worth noting that ASPERA-3 usually does not detect (probably owing to the limited coverage of the unit sphere by the IMA spectrometer) cold heavy planetary ions which are expected from the deviations between the electron densities measured by MARSIS and ASPERA-3 within the magnetic barrier in the subsolar sheath. However, in
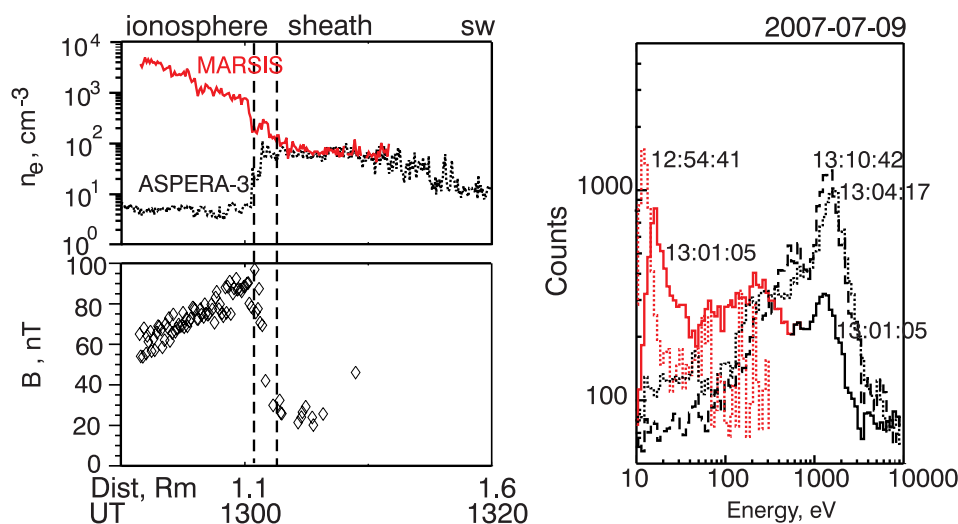

Figure 4. (left, top) Variations in the electron number density measured by ASPERA-3 and MARSIS, and (left, bottom) the magnetic field strength across the MPB. (right) Ion spectra measured by ASPERA-3 within the MPB crossing (1301:05 UT) and in the adjacent magnetosheath (1304 and 1310 UT) and ionosphere (1254 UT). Spectra of solar wind and planetary ions are shown by black and red, respectively. Vertical lines show the width of the transition.
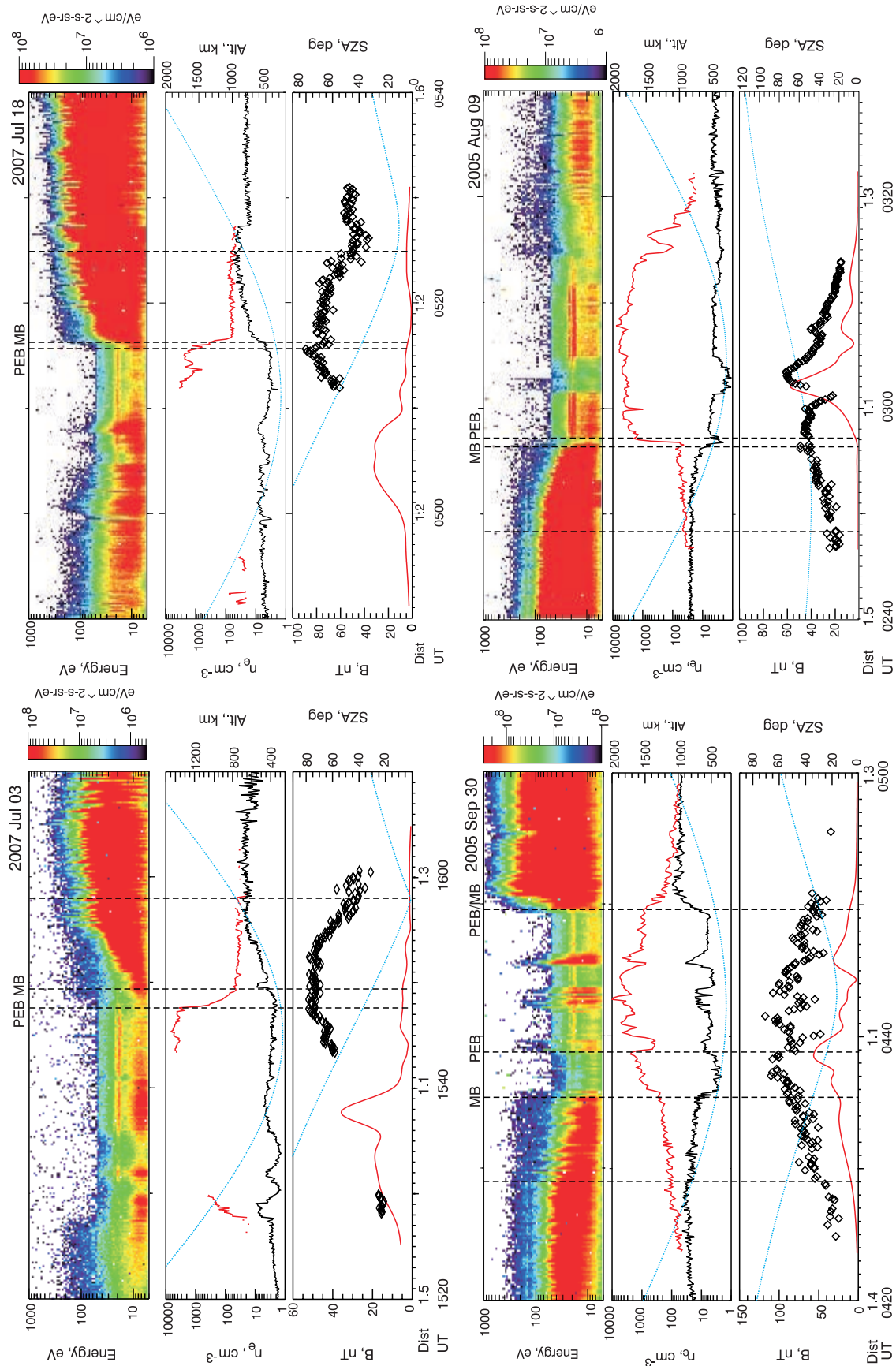
Figure 5. Examples of the ASPERA-3 and MARSIS observations in the subsolar region. Vertical dashed lines without a label mark the onset of the magnetic field pileup. The format is the same as in Figure 1.
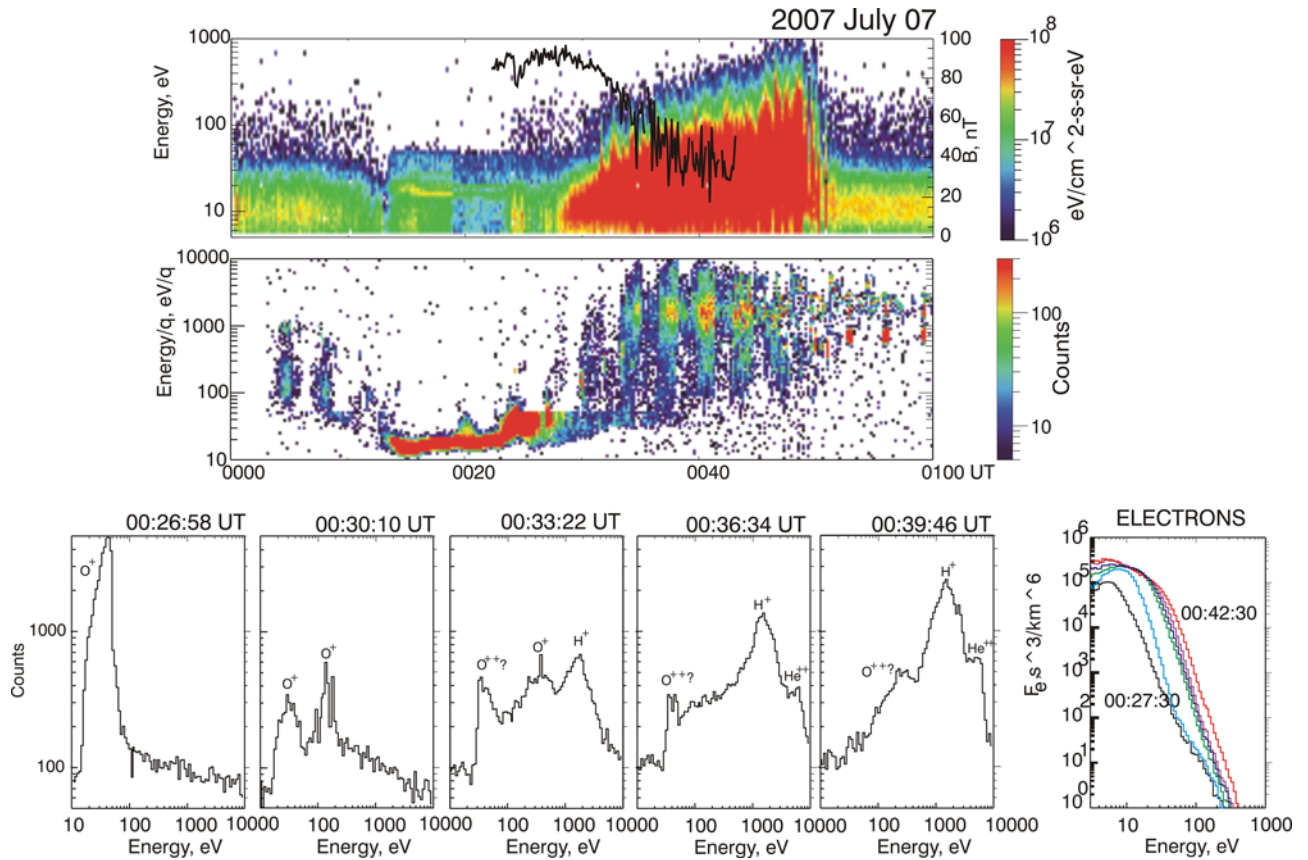
Figure 6. (top) Energy-time spectrogram of the electron fluxes with the imposed curve of the magnetic field value. (middle) Energy-time spectrogram of the ion fluxes. Two different ion populations (solar wind and planetary plasmas) are mixed in the magnetic barrier region. (bottom) Evolution of ion spectra and electron distribution functions (the right panel in the bottom row depicts the electron distributions with 3 min interval) across the magnetic barrier.

some cases such data are available. Figure 6 presents an example of the measurements. The curve of the magnetic field intensity determined from MARSIS data is superimposed on the energy-time spectrogram of electron fluxes. The middle panel presents the energy-time spectrogram of ion fluxes. All ion species are included. The dense ionospheric component (mainly oxygen ions) with $E \leq 50$ eV observed on the ion spectrogram at 0014–0027 UT spreads to the magnetosheath where it is mixed with plasma of the solar wind origin (0028–0038 UT). A gradual energization of oxygen ions with the distance to Mars indicates that some part of the momentum flux is transferred from solar wind to planetary plasma. Spectra of electrons and ions measured at different time intervals are also shown in the bottom panel. At 0026 UT, when MEX is clearly inside the ionosphere, the IMA sensor measures cold oxygen ions. Close to the magnetospheric boundary (∼0030 UT) two populations of oxygen ions, the ionospheric component and ions accelerated up to ∼100 eV, are observed. At 0033 UT a mixture of solar wind protons and oxygen ions indicates a mass-loading process. Peaks corresponding to $m/q = 8$, which could be a signature of O^{++} ions, are also detected. Electron spectra show a gradual depletion of more energetic particles while moving from the magnetosheath to the magnetosphere. Such an evolution of the electron spectra could be due to energy losses on impact ionization.

[14] It is also observed (Figure 5) that the magnetosheath/ionosphere interface between the MB and PEB is filled by a dense plasma and the topside ionosphere is magnetized. Energy characteristics and ion composition in this region are better resolved by ASPERA-3 at larger solar zenith angles (see, e.g., Figure 9). The width of the interface in the subsolar region varies and can be very narrow (few tens km in the altitude). Sometimes the positions of the MB and PEB almost coincide.

[15] Figure 7 (left) compares the solar wind dynamic pressure $\rho V^2 \cos^2(SZA)$, where ρ, V and SZA are, respectively, the mass density, bulk velocity and the solar zenith angle at the time of the MB crossing, and the magnetic field pressure $B^2/8\pi$ at the MB for several orbits crossing the MB in the subsolar region. Solar wind parameters and the magnetic field strength were determined from the ASPERA-3 and MARSIS data, respectively. The SZA was taken from the MB location [see *Dubinin et al.*, 2008b]. The magnetic field value grows up to the values just sufficient to balance the solar wind pressure. Figure 7 (right) shows with triangles the altitude of the MB as a function of solar wind dynamic pressure for the same data set. Although the ram pressure varies by a factor 5–6 the position of the MB remains approximately in the same altitude range (450–550 km). It is interesting to note that a rise of the induced field to take up the pressure balance was found at Venus
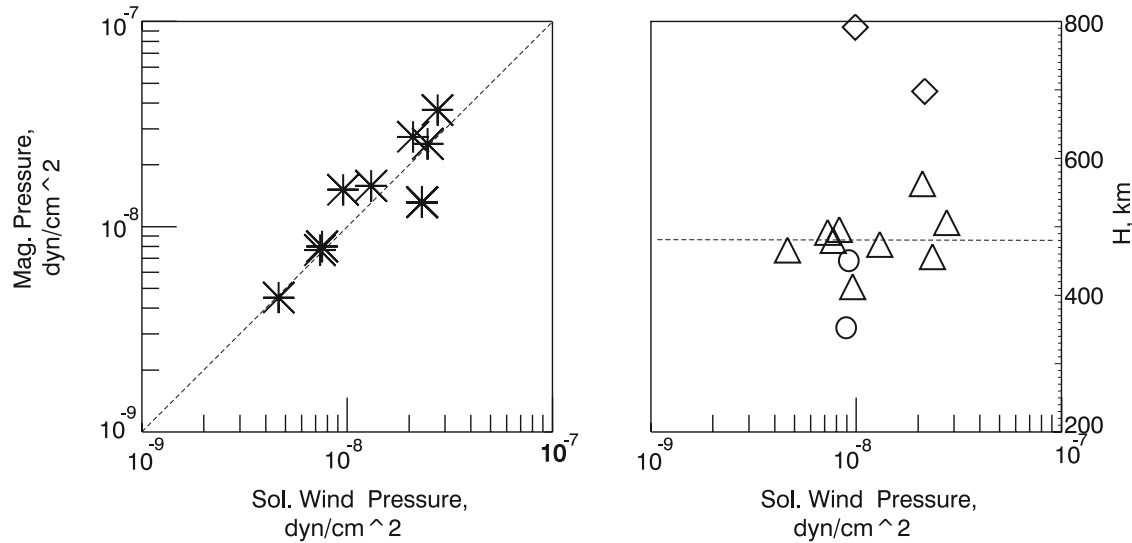
Figure 7. (left) Magnetic field pressure at the MB versus the solar wind dynamic pressure for several MEX orbits crossing the magnetospheric boundary in the subsolar region. (right) Altitudes of the MB as a function of the solar wind pressure are shown as triangles. Diamond symbols correspond to the orbits above local crustal magnetizations (see Figures 8a and 8b). Circles correspond to the MB positions for crossings without the magnetic field pileup (see Figures 8c and 8d).

under high solar wind dynamic pressure conditions when the Venusian ionosphere becomes magnetized [see, e.g., *Luhmann and Cravens*, 1991].

3.2. Crossings of the MB Above Crustal Sources

[16] Spikes of magnetosheath plasma within the ionosphere measured from the orbit on 30 September 2005 at ∼0439:30, 0442:30 and 0445:30 UT (Figure 5) could be signatures of the plasma protrusion through the cusps of minimagnetospheres formed by the solar wind interaction with the local crustal sources (the value of the undisturbed crustal field reaches ∼50 nT in this region). Enhancements in plasma density of the hot component (E_e > 5 eV) are commensurate with drops in the number density of the ionospheric plasma measured by MARSIS. This is probably due to easier vertical transport of the ionospheric plasma in the regions where the radial magnetic field prevails. However, the electron spikes observed by ASPERA-3 and the corresponding dropouts in the magnetic field strength could be also signatures of the current sheets arising owing to strong local draping of the magnetic field lines inside the ionosphere or owing to reconnection between the IMF and crustal field lines. It will be shown below that such structures are also accompanied by a dropout in the density of the cold ionospheric component.

[17] The MB altitude significantly increases above the planetary regions with strong crustal magnetizations [see also *Dubinin et al.*, 2008a]. The diamond symbols in Figure 7 (right) depict the MB position for two such crossings. The position is shifted upward to the altitudes of 700–800 km. The data for these orbits are presented in Figures 8a and 8b. The third panels from the top show the magnetic field value (diamonds). The solid blue and red curves depict the model magnetic field strength and the vertical component of the crustal field, respectively. The bottom panels show the magnetic field pressure (dia-

monds) and the thermal ionospheric pressure $n_e kT$, where $T = T_e + T_i = 1$ eV (blue curves). The dashed red curves give the idea of the solar wind dynamic pressure measured by ASPERA-3 in the solar wind. Although the MB crossings are characterized by a sudden jump in n_e, the thermal pressure of the cold plasma is not sufficient to balance the solar wind ram pressure. On the orbit on 13 July (Figure 8a) the magnetic field in the magnetosheath increases producing the magnetic barrier for solar wind plasma. Since it is difficult to distinguish between the IMF and crustal field without measurements of the field components we cannot say definitely whether the Earth-type magnetopause is formed or both factors, a pileup of the IMF and compression of the crustal magnetic field, provide us with a larger scale to the magnetospheric obstacle. Closer to the planet the magnetic field is dominated by local sources. Drops in the density of the ionospheric plasma measured by MARSIS at ∼1049 UT, 1100 UT and 1003 UT are observed in the regions with strong vertical magnetic field component of crustal sources. On the orbit on 10 July (Figure 8b), the magnetic field in the inner magnetosheath also increases but does not reach the value which is sufficient for a pressure balance. The growth of the magnetic field value in the barrier is followed by a sudden drop at 0913 UT. Such a diamagnetic cavity can be easily created owing to a plasma heating of the ionospheric component (∼1.5 eV). It is interesting to note that a similar, although a smaller cavity, is also observed on 13 July. As for the orbit on 13 July, dropouts in the electron density at 0905 UT and 0907:30 UT are observed in the regions with strong model vertical magnetic fields.

[18] The boundary of photoelectrons (PEB) can be closer to the planet as on 13 July or coincide with the MB as on the orbit on 10 July. Spikes of the electrons at ∼1103 UT (13 July) and at 0907:30 UT (10 July), which are observed
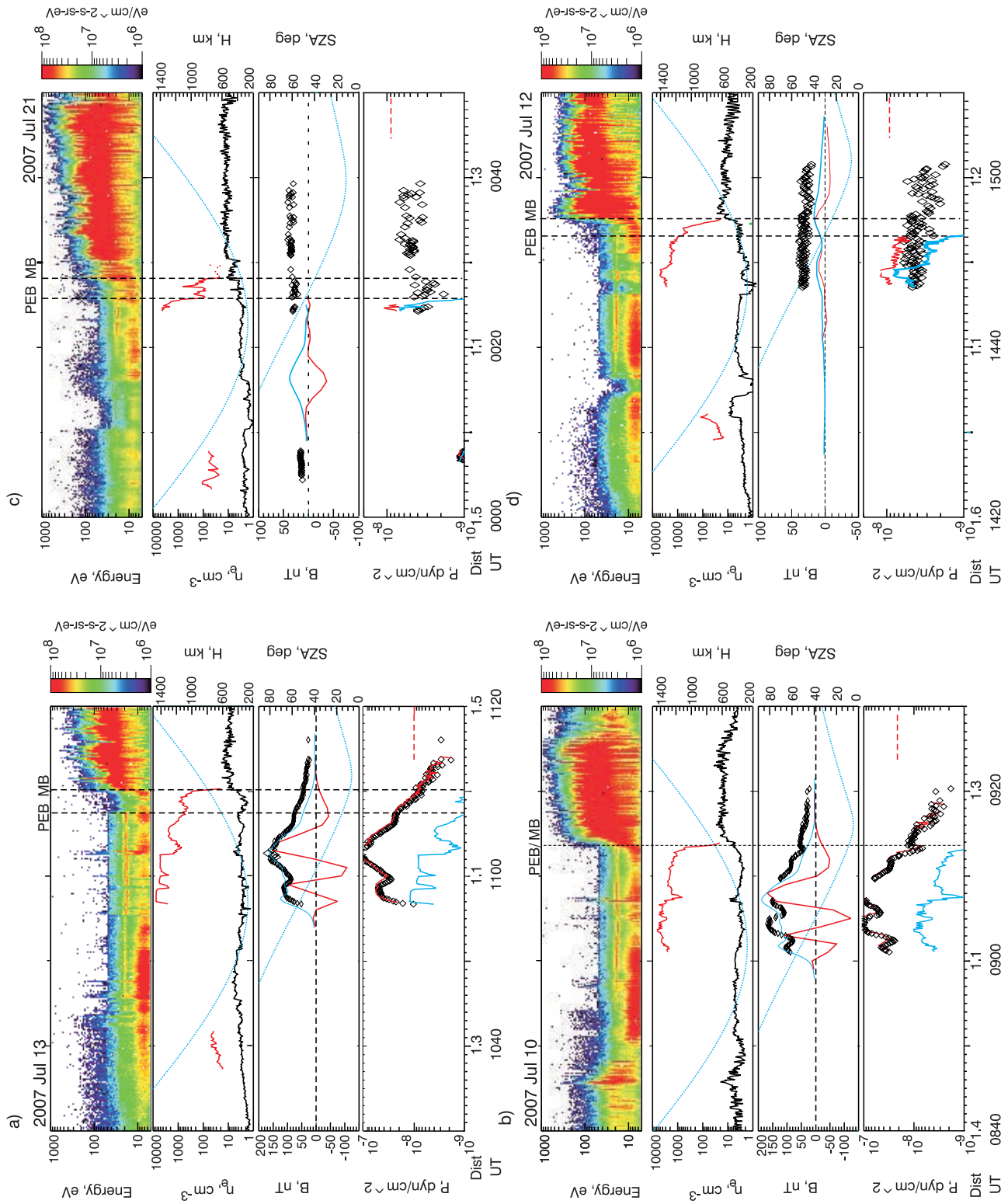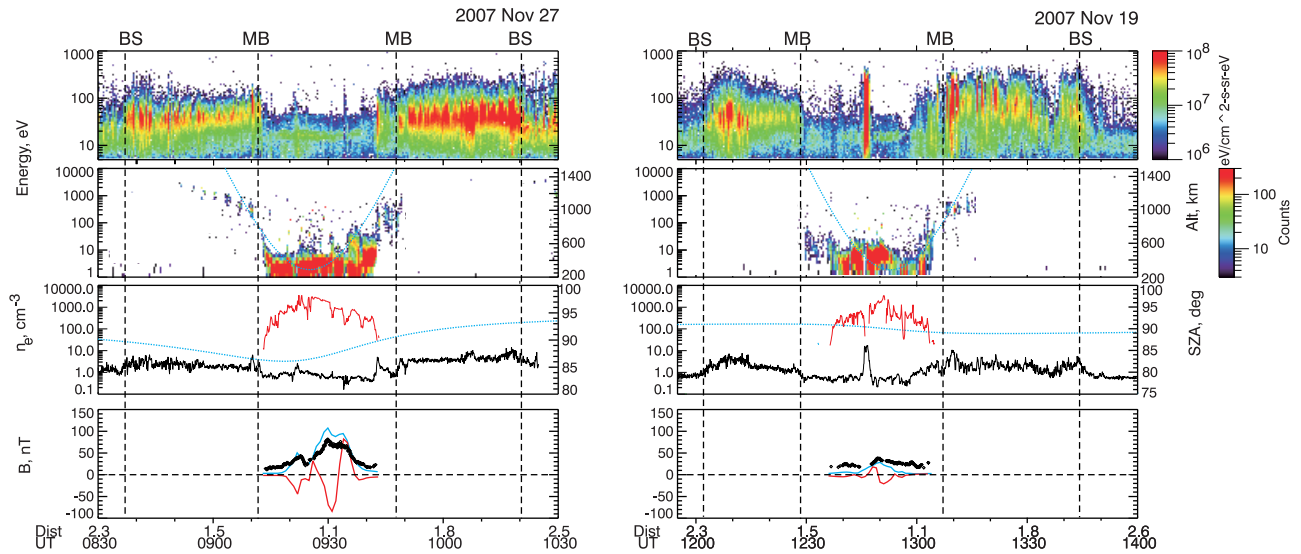
Figure 8

Figure 9. Observations from the MEX orbits close to the dawn-dusk plane. From top to bottom: energy-time spectrogram of electron fluxes; spectrogram of ion ($m/q > 16$) fluxes; electron number densities measured by ASPERA-3 (black) and MARSIS (red); and the magnetic field strength from the observations (diamonds) and the model (blue curve); the red curve shows the vertical component of the model crustal field. The spacecraft altitude and the solar zenith angle are shown by blue dotted curves on the second and third panels with axes on the right.

in the region of strong radial crustal field, probably correspond to weak plasma injections along the open field lines. As in the case of the orbit on 30 September, 2005 (Figure 5) the "injections" of the magnetosheath electrons are accompanied by drops in the density of the ionospheric component which dominates in this region.

3.3. Absence of the Magnetic Barrier

[19] In some cases the crossings of the Martian magnetosphere on the dayside occur without a signature of a magnetic field pileup. Figures 8c and 8d present examples of such crossings. On the orbit on 12 July the MB is rather sharp with an abrupt increase in the total electron number density inferred from the MARSIS measurements. The magnetic pressure still dominates although the balance is achieved only at the PEB with contributions of both pressure terms. On the orbit on 21 July, the transition from the sheath to the ionosphere is smoother. In the interface region between the MB and PEB the behavior of the total electron density is rather irregular. Peaks in n_e are accompanied by the diamagnetic drops in the magnetic field pressure. Inside the PEB ($\sim$0024:30 UT on 21 July; 1447–1449 UT on 12 July) the thermal pressure of the ionospheric component prevails over the magnetic pressure. The altitude of the MB for these two crossings is shown in Figure 7 (right) by circles. On the orbit on 21 July, the altitude is less ($\sim$350 km) as compared to the cases when the magnetic barrier is formed. The MB crossings without the field draping may occur in the hemisphere which is

opposite to the hemisphere into which the motional electric field ($\mathbf{E}_{mot}$) points. Indeed, previous observations and simulations [Vennerstrom et al., 2003; Modolo et al., 2006] show a clear asymmetry of the magnetic field in both hemispheres.

3.4. Terminator Region

[20] Figure 9 shows data for the MB crossings near the terminator. The spacecraft was moving near the dawn-dusk meridian. Positions of the bow shock (BS) and the magnetosphere boundary (MB) are shown by the vertical dashed lines. The two top panels present spectrograms of electron fluxes and heavy ($m/q > 16$) planetary ions. A shift of the energy peaks of CO_2 photoelectrons allows estimation of the spacecraft potential ($V_{s/c} \sim -8$ to -9 V) and adjustment of the energy of the IMA spectrometer, accordingly. The third panels from the top depict the electron number density measured by ASPERA-3 (the black curves) and MARSIS (the red curves). Most part of the magnetosphere which is void of solar wind plasma is filled by cold ionospheric plasma. The ionospheric plasma expands up to altitudes >1000 km near the terminator. Closer to the MB, the energy of planetary ions increases. This region (boundary layer or mantle) is the counterpart of the interface between the sheath and ionosphere on the dayside. Further in the magnetosheath, the energy of planetary ions gradually increases. This is a typical pickup population controlled by the IMF direction. On the orbit on 27 November, pickup ions are observed on the inbound leg (0850–0910 UT)

Figure 8. (a and b) Crossings above strong crustal sources on Mars. In addition to the parameters shown in Figure 4 the radial component of the model crustal field is added in the third panel (red). The fourth panel contains the magnetic field pressure (diamonds), thermal pressure of the cold ionospheric component (blue), total pressure (red), and the ram solar wind pressure (dashed red). (c and d) Crossing without a pileup signature.
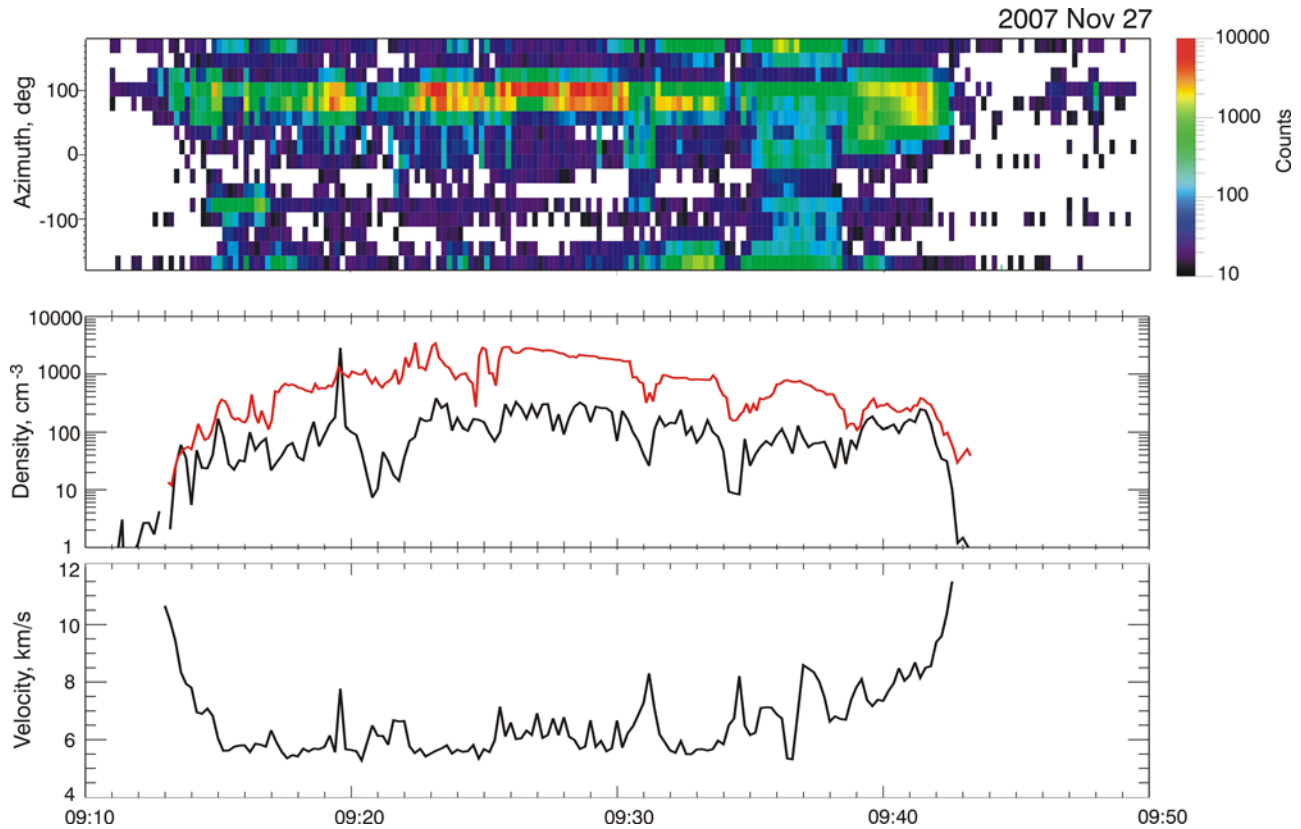
Figure 10. (top) Arrival angle-time spectrogram of low-energy ions measured close to the terminator. (middle) Total electron density from MARSIS (red curve) and the number density of oxygen ions with $E_e \leq 50$ eV evaluated from the ASPERA-3 data. (bottom) Velocity of oxygen ions with $E_e \leq 50$ eV.

while on the orbit on 19 November, they are measured on the outbound leg (1308–1315 UT).

[21] It is important to note that the low-energy/cold ions measured by ASPERA-3 in the region where MARSIS records large electron number densities have a rather narrow angular distribution indicating their bulk motion. Figure 10 (top) shows variations in the flux of low-energy planetary ions ($E \leq 50$ eV) as a function of time and the azimuth angle of the ion instrument for the orbit occurring on 27 November 2007. Ions are coming from the angle $\sim 100°$ that approximately corresponds to antisunward motion. The measurements were made without scanning in the elevation (θ) direction and covered only the field of view of $5° \times 360°$. Assuming that the angular distribution of ion fluxes in the θ direction is similar to their distribution in the azimuth (φ) direction, one can estimate the ion number density from the moment calculations. The middle panel compares the number density of low-energy oxygen ions (the black curve) and the total electron density from the MARSIS observations (the red curve). Both instruments often record the same small-scale structures. The bottom panel shows the bulk ion speed evaluated from the ion peak energy of their distribution functions. Notwithstanding some uncertainties related with the ASPERA-3 ion measurements at low energies (the spacecraft potential, two-dimensional measurements, uncertainties in the energy settings and in the geometric factor) it is evident that the observed efficient momentum transfer from the solar wind to the top ionosphere could be an important mechanism for

solar wind induced escape of planetary matter [*Lundin et al.*, 2008]. However, whether the whole ionospheric plasma at these altitudes is driven into motion by the solar wind or only its suprathermal part gets driven into motion remains unknown.

[22] Another interesting feature is large-amplitude (at one order of magnitude) variations in the number density of the cold component (Figure 9). As in the previous examples, the appearance of ionospheric "holes" (27 November, 0931 UT and 0934 UT) correlate with the peaks in the vertical component of the crustal magnetic field (the total value and the vertical component of the model crustal field are shown on the fourth panel by the blue and red curves, respectively) indicating an easier escape of the ionospheric electrons to space along the open field lines. On the other hand, similar dropouts in the ionospheric density are observed on the orbit on 19 November, where the role of the local crustal sources is insignificant. Note here that a structured ionosphere was also often observed on another unmagnetized planet, Venus [*Brace et al.*, 1980, 1983]. Among possible mechanisms of large-scale oscillations we mention a shear driven instability due to interaction with the solar wind [*Duru et al.*, 2008] or the modified Rayleigh-Taylor instability proposed to explain the appearance of the large-amplitude striations in the artificial comet AMPTE [see, e.g., *Bingham et al.*, 2000].

[23] Another interesting feature is a narrow spike of electrons with spectra typical for the plasma sheet and with a coincident drop in the density of the cold ionospheric
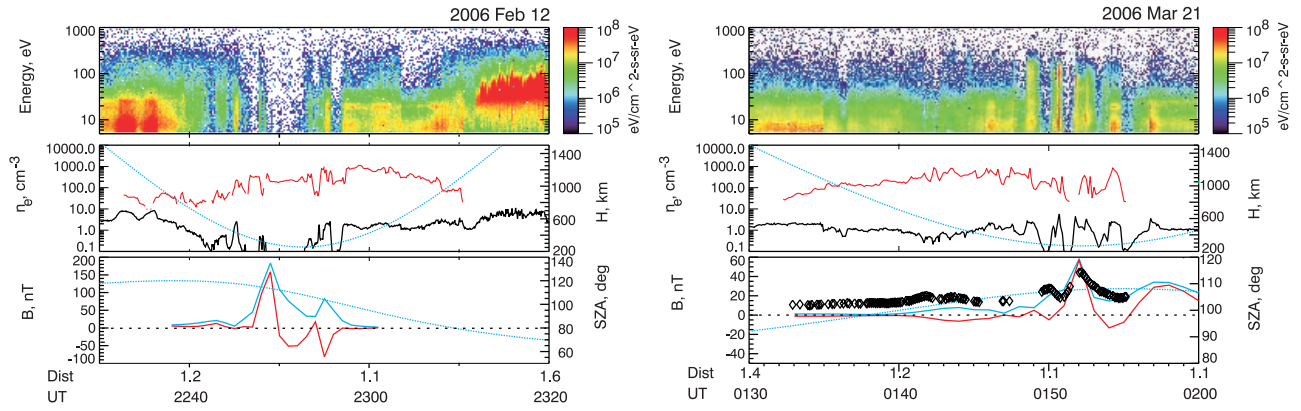
Figure 11. The ASPERA-3 and MARSIS data from the observations on the nightside. The same plot setup as for Figure 1. The blue (red) curves on the bottom panels show the value and vertical component of the model crustal field. There are no field data from MARSIS on the orbit on 12 February 2006.

component observed at 1246 UT on 19 November. Similar effects are typical for the crossings of the plasma sheet at low altitudes, within the ionosphere, which shows the existence of strong erosion processes in such regions. The erosion is maintained by the enhanced transport of ionospheric plasma by $j \times B$ forces.

3.5. Nightside

[24] Figure 11 shows examples of the observations in the night sector when MEX entered the optical shadow of Mars. The dayside ionosphere easily identified on the electron spectrograms by the photoelectron "peaks" terminates at SZA $\sim 100°$. However, the MARSIS data show that the topside ionosphere also exists at higher zenith angles and even in the shadow region. It is observed that the regions almost void of solar wind plasma often contain an ionospheric component with densities ≥ 100 cm^{-3}. Narrow spikes of suprathermal electrons seen on the spectrograms of electron fluxes are commonly topologically related with open field lines whose foots are in the region of strong crustal sources. They form narrow strips in areas with strong upward or downward crustal magnetic field and can explain the observed auroral UV emissions [Dubinin et al., 2008a, 2008c; Leblanc et al., 2008]. A downward flux of particles can also ionize the Martian atmosphere providing the spots

with enhanced ionization. This effect has been recently observed by Safaeinili et al. [2007]. Here we present examples when spikes of sheath-like electrons correlate with depletions in the total electron density ($\sim$2248 UT and $\sim$2256 UT on 12 February 2006).

[25] Another class of electron distributions which contains peaks at $E_e \geq 80 - 100$ eV was observed at 0150:30 UT and 0151:40 UT on 21 March 2006. Such peaked distributions might be signatures of inverted V structures on Mars and can be related to upward field-aligned currents and electric field potential drops on Mars [Brain et al., 2006; Lundin et al., 2006; Dubinin et al., 2008d]. It is observed that these events are also accompanied by dropouts in the electron density of ionospheric plasma. Note that the appearance of small cavities on the auroral field tubes on Earth is rather similar and caused by plasma evacuation along the field lines.

4. Discussion

[26] Simultaneous measurements of the cold planetary plasma and warm solar wind plasma performed by the MARSIS and ASPERA-3 experiments on Mars Express allow us to better comprehend the plasma environment of Mars. Figure 12a shows the combined map of the maximum
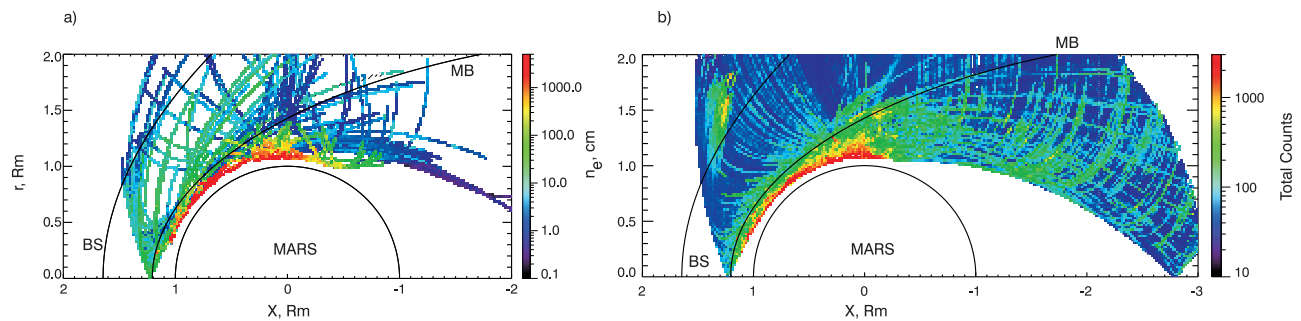

Figure 12. (a) Map of the electron number density measured by ASPERA-3 and MARSIS on $\sim$90 MEX orbits with simultaneous observations. The data are given in cylindrical coordinates X_{MSO}, $r = (Y_{MSO}^2 + Z_{MSO}^2)^{1/2}$. The average positions of the bow shock and the magnetospheric boundary are also shown [Dubinin et al., 2006b]. (b) Map of the distribution of the cold heavy planetary ions measured by ASPERA-3 in May–December 2007.

electron number density in each bin from the ASPERA and MARSIS data set. Although the solar wind is terminated rather far from the planet, it gets in touch with the dense planetary plasma of ionospheric and exospheric origin at the dayside. At solar zenith angles $\geq 80°$ the number density of the ionospheric plasma rapidly decreases. Note that the MARSIS measurements were made only at the altitudes less than 1300 km. In fact, cold/low-energy ionospheric plasma is forced to expand toward the tail at much larger distances that is confirmed by the ASPERA-3 measurements. Figure 12b presents the map of the distribution of cold planetary ions measured by the IMA sensor for $m/q \geq 16$ and $E/q = 10–50$ eV in cylindrical coordinates. The map shows the mean values of the measured total counts in each $0.02 \times 0.02\ R_m$ bin. Although ion fluxes decrease near the terminator, a significant amount of cold ion population can be found far in the tail. The picture is very similar to the well-known sketch of the Venusian ionosphere [*Brace et al.*, 1987]. A scavenging process is accompanied by a gradual ion energization in electric fields of the different origin.

[27] Electric currents flowing in the interface region between both plasmas induce the magnetosphere which is almost void of solar wind. The structure of the induced magnetosphere of Mars on the dayside can vary substantially. In a common case, the IMF carried by solar wind is piled up in the inner part of the magnetosheath. As a result, the magnetic field pressure balances the incident solar wind dynamic pressure and an induced magnetospheric boundary is formed. At first glance, the structure of the magnetic barrier resembles the plasma depletion layer (PDL) observed near the Earth magnetopause (plasma depletion due to a squeezing along the field lines and an enhanced transport transverse to the magnetic field under the magnetic field tangential stresses is compensated by the magnetic field increase). However, the fundamental difference is that the total plasma density in the magnetic barrier increases. Although the density of the solar wind plasma decreases, while approaching the MB from outside, plasma of planetary origin begins to prevail and contributes to the total increase in the electron plasma density. It is worth noting that the thermal plasma pressure still decreases and the magnetic pressure dominates. Such a picture emerges from the comparison between variations in the total electron density measured by MARSIS and the electron density of the solar wind plasma recorded by ASPERA-3. The electron population of the magnetosheath plasma is gradually depleted by more energetic electrons while the magnetic field intensifies within the magnetic barrier. The spatial evolution of energy spectra of solar wind electrons hints at an important role of impact ionization in the formation of the magnetic barrier.

[28] The measurements by MARSIS of a very extended "ionosphere" with rather large number densities in the dayside magnetosheath correspond to periods of a dense solar wind measured by ASPERA-3. On the other hand, the plasma detected by MARSIS in the inner sheath is not only of solar wind origin since $\Delta n_e = n_{e,Marsis} - n_{e,Aspera}$ increases toward the planet. Both factors indicate that plasma in the magnetic barrier with the density of $\sim \Delta n_e$ is not a photoplasma, but probably originates owing to charge exchange and impact ionization processes, the efficiency of which is linearly proportional to the solar wind density. However, there is, at least, one serious problem in

such a scenario. Except for rare cases, as, for example, on 7 July 2007 (Figure 6), the IMA sensor does not detect cold/low-energy planetary ions in this region that could be, for example, either due to the restricted field of view of the ion sensor or hints at another mechanism of the barrier formation. It is also worth mentioned that protons with energies less than several hundreds eV are not measured by the IMA sensor. This constraint does not allow evaluation of an efficiency of charge-exchange of solar wind protons.

[29] Note here that an enhanced draping around an impenetrable blunt obstacle can be also described in terms of standard gasdynamic models assuming that the obstacle boundary is a tangential discontinuity [*Spreiter et al.*, 1970; *Luhmann et al.*, 1986]. In fact, this gasdynamic convecting model is not self consistent since the magnetic field is imposed onto the gasdynamic solutions using the frozen-in condition. Then the field tubes convecting very slowly through the stagnation region where the velocities are small are strongly piled up and the field strength can become infinitely large unless the density goes to zero. The MHD models [see, e.g., *Ma et al.*, 2004], include the magnetic field self-consistently. A slowdown of plasma and formation of the magnetic barrier due to a mass loading of solar wind on planetary plasma was clearly observed by *Ma et al.* [2004].

[30] An important feature of the observations is that the magnetic field in the barrier rises up to the value which is just sufficient to balance the solar wind pressure while the position of the magnetospheric boundary varies insignificantly. Thus, the process of the barrier formation is governed by solar wind. Such a coupling can be understood in the terms of "heavy mass loading" suggested by Haerendel in the work of *Szego et al.* [2000]. Planetary ions which on such scales are not magnetized owing to their large mass experience only the motional electric field $-V \times B$, and the magnetic field is set up by the Hall current of the drifting in the $E \times B$ electrons. The electrons carrying the integrated Hall current in this layer are neutralized by the solar wind protons implying $J_H = cB/4\pi \approx en_{sw}V_{sw}L$, where L is a characteristic width of the boundary layer estimated as $1 \div 2c/\omega_{pi}$. Then, using $\omega_{pi} = (4\pi n_e e^2/m_p)^{1/2}$ the magnetic field jump is easily evaluated as $B \sim \sqrt{8\pi\rho_{sw}V_{sw}^2}$ ($\rho_{sw} = n_{sw}m_p$; m_p is the proton number density) which is in agreement with the observations. It is interesting to note that the processes of ion extraction from the ionosphere and the barrier formation are coupled in this model via the solar wind parameters. Another possible mechanism is that the magnetic barrier is created by the Chapman-Ferraro currents carried by solar wind electrons, similar to what happens at an Earth-type magnetopause. Then one can also expect the fulfillment of the pressure balance condition $B^2/8\pi \approx \rho V^2$. In such a model, the magnetic field, at which impinging solar wind particles are reflected, must be decoupled from solar wind (e.g., it could be the magnetic field induced by ionospheric currents at closer distances). However, it is difficult to explain in terms of this model, a gradual depletion of more energetic electrons.

[31] There are also cases when a pileup of the magnetic field occurs in a rather narrow layer and looks like a discontinuity. Such a transition, called the magnetic pileup boundary (MPB), is also characterized by a jump in the total electron density and by a mixture of the solar wind and
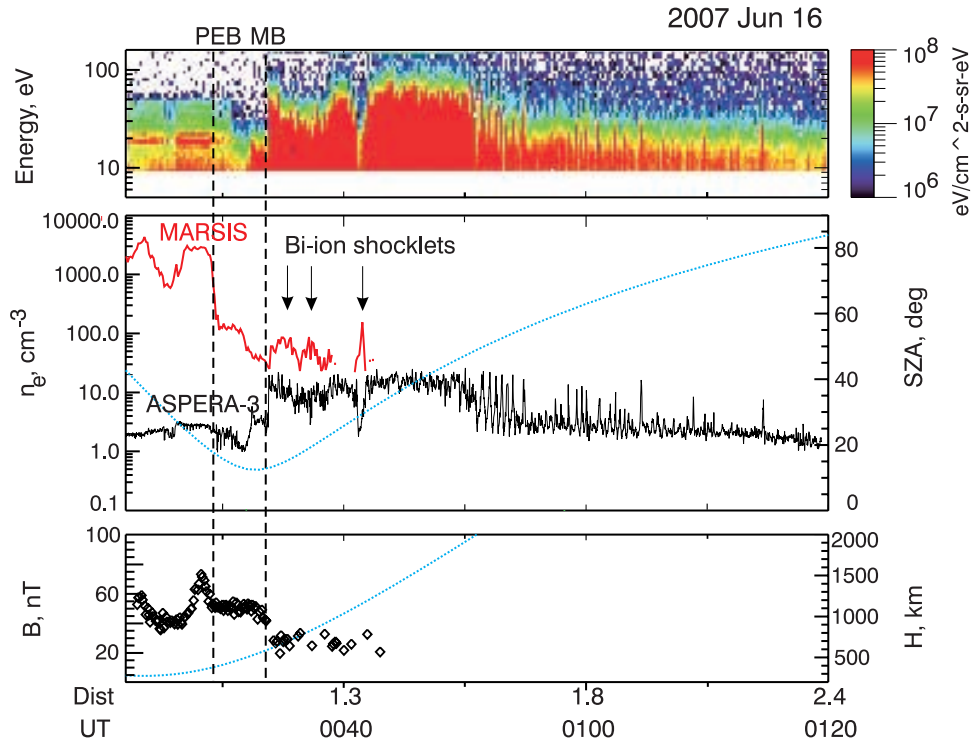
Figure 13. (top) Spectrogram of electron fluxes, (middle) electron number densities evaluated from MARSIS and ASPERA-3 data, and (bottom) magnetic field strength from MARSIS. The different behavior of the solar wind and planetary plasmas is a probable manifestation of bi-ion effects.

planetary plasmas. Probably we observe a regime of mass loading when the loading by the planetary plasma becomes so strong that the ambient flow is completely stopped [*Szego et al.*, 2000]. Note that there were also attempts to consider the magnetic pileup boundary as a "heavy ion shock" in multi-ion plasma [*Sauer and Dubinin*, 2000; *Dubinin et al.*, 2006a]. The interesting feature of such type of shocks is a different behavior of the protons and heavy ions. Deceleration and compression of heavies may occur along with acceleration and rarefaction of protons. Such intermittent plasma structures with dominance either by protons or heavies (bi-ion shocklets) are predicted by the theory of multi-ion flows [*Dubinin et al.*, 2006a]. Sometimes, similar structures are observed in the subsolar magnetosheath. Figure 13 shows an example of observations occurring when jumps in the density of the planetary plasma, recorded by MARSIS in the sheath (0035 UT, 0037 UT and 0041 UT), are accompanied by rarefactions in solar wind plasma (ASPERA-3) and precede the main MB transition (compare with Figures 12 and 15 of *Dubinin et al.* [2006a]). Dropouts of solar wind electrons are also well seen on the energy-time spectrogram shown on the top panel.

[32] The MARSIS and ASPERA-3 observations also reveal a transition across the magnetospheric boundary without a pileup. We suppose that such a distribution can appear in the hemisphere out of which the motional electric field of the solar wind points. Hybrid simulations by *Modolo et al.* [2006] show that a pileup of the magnetic field is clearly observed in the E^+ hemisphere and almost absent in the E^- hemisphere. The simulations also show that

in the E^- hemisphere solar wind plasma is able to reach lower altitudes where charge-exchange processes are more efficient (R. Modolo, private communication, 2008). As a result, a part of the momentum flux carried by solar wind protons is lost that influences a pressure balance.

[33] Inside the magnetospheric boundary, the electron density continues to increase reaching $\sim 3 \cdot 10^3$ cm^{-3} at the photoelectron boundary. The absence of CO_2-peaks on the electron energy spectra in the interface region between the magnetosheath and the ionosphere shows that the plasma population here has another origin or composition. The magnetic field intensity also often increases in this region implying a convective field transport by the planetary plasma driven into global motion.

[34] The existence of a sharp photoelectron boundary is another important feature. It is expected that the boundary is gentler in the E^+ hemisphere into which the motional electric fields points and sharper in the opposite E^- hemisphere. In the E^+ hemisphere, where the motional electric field is directed radially outward, planetary ions are extracted while in the E^- hemisphere, where the electric field is directed inward, ionospheric ions experience a force preventing their expansion. At lower altitudes the magnetic field tangential stresses associated with a strong enhancement in the draping of the field lines at the MB [*Bertucci et al.*, 2003] begin to dominate producing a sharp PEB even in the E^+ hemisphere. These forces act on the ionospheric ions by means of an inward pointing ambipolar electric field while the electrons experience the $j \times B$ force. It is more difficult to explain the existence of a rather sharp PEB where there is no a significant pileup of the magnetic field

(see, e.g., Figures 8c and 8d). The inward directed electric field in the E^- hemisphere and charge-exchange processes which reduce the thermal pressure of the magnetosheath protons are probably the main processes.

[35] Near the terminator, in the sheath/ionosphere interface planetary ions gain energies up to ≤ 1 keV which is close to the typical proton energy in the adjacent magnetosheath. Under a favorable geometry of the MEX orbit with respect to the motional electric field, ASPERA-3 can record planetary oxygen ions and their further energization in the magnetosheath. This is a classical pickup population (see, e.g., Figure 9). However, the most part of the energized planetary heavy ions forms a boundary layer/mantle and plasma sheet.

[36] The cold/low-energy population (at least, the suprathermal component measured by ASPERA-3) at the altitudes explored by MEX is also not in a static equilibrium, but is driven into the bulk convective motion. This is confirmed as well by the ASPERA-3 measurements, and by the MARSIS observations of nearly constant density of the ionospheric plasma at low altitudes at $SZA \leq 80°$ [*Duru et al.*, 2008]. The latter can be explained by a horizontal transport of plasma from the dayside. Such a tailward comet-like expansion of cold plasma with further energization can essentially increase the nonthermal loss rates of the ionospheric components on Mars [*Lundin et al.*, 2008].

[37] The ionospheric plasma often reveal large-amplitude oscillations in the number density recorded by both instruments. These oscillations could be a result of shear or other fluid-like plasma instabilities. It is worth noting that a corrugated shape of the topside ionosphere on Mars resembles large-scale density perturbations in the AMPTE experiments with *Ba*-releases in the solar wind [*Valenzuela et al.*, 1986; *Haerendel et al.*, 1986]. It is observed that some depletions in the density correlate with large vertical components of the crustal magnetic field. The magnetic field lines threading such troughs are probably open and the ionospheric electrons can easily escape to space. Local depletions of the ionosphere are also observed in the plasma sheet which is well traced by spikes of magnetosheath-like electrons (*Dubinin et al.*, 2006c). The draped field lines slipping around the "magnetic poles" push out the ionospheric plasma. It is supposed that the depletion is caused by a significant increase in the velocity of plasma transport due to the $j \times B$ force. A probable counterpart of such structures on Venus is "ionospheric holes" observed by the PVO spacecraft [*Brace et al.*, 1982].

[38] At $SZA \geq 80°$, where the transition to the nightside occurs, the ionospheric density decreases very rapidly. An abrupt drop of CO_2 photoelectrons is also often observed close to the terminator. Although the nightside ionosphere is almost void of solar wind electrons the total electron number density in this region is about $100-200$ cm^{-3} at ~ 300 km altitude. Spikes of suprathermal electrons and peaked electron distributions observed in the regions with strong crustal fields, which are often regarded as a source of aurora on Mars [*Brain et al.*, 2006; *Lundin et al.*, 2006; *Dubinin et al.*, 2008a, 2008c, 2008d; *Leblanc et al.*, 2008], correlate rather with the density depletions than with density enhancements. Note here that auroral flux tubes on Earth are often plasma depleted owing to enhanced ion evacuation. Probably similar processes operate on Mars as well.

References

Acuña, M., et al. (1998), Magnetic field and plasma observations at Mars: Initial results of the Mars Global Surveyor MAG/ER experiment, *Science*, *279*(5357), 1676.

Barabash, S., et al. (2006), The analyzer of space plasma and energetic atoms (ASPERA-3) for the Mars Express mission, *Space Sci. Rev.*, *126*, 113.

Bertucci, C., et al. (2003), Magnetic field draping enhancement at the Martian magnetic pileup boundary from Mars Global Surveyor observations, *Geophys. Res. Lett.*, *30*(2), 1099, doi:10.1029/2002GL015713.

Bertucci, C., C. Mazelle, M. H. Acuña, C. T. Russell, and J. A. Slavin (2005), Structure of the magnetic pileup boundary at Mars and Venus, *J. Geophys. Res.*, *110*, A01209, doi:10.1029/2004JA010592.

Bingham, R., R. Bollens, F. Kazeminejad, and J. M. Dawson (2000), Simulation studies of the interaction of a neutral gas and flowing plasma, in *Cometary Plasma Processes, Geophys. Monogr. Ser.*, vol. 61, edited by A. D. Johnstone, pp. 73–85, AGU, Washington, D. C.

Brace, L. H., R. F. Theis, W. R. Hoegy, J. H. Wolfe, J. D. Mihalov, C. T. Russell, R. C. Elphic, and A. F. Nagy (1980), The dynamic behavior of the Venus ionosphere in response to solar wind interactions, *J. Geophys. Res.*, *85*, 7663.

Brace, L. H., R. F. Theis, H. G. Mayr, S. Curtis, and J. Luhmann (1982), Holes in the nightside ionosphere of Venus, *J. Geophys. Res.*, *87*, 199.

Brace, L. H., R. C. Elphic, S. A. Curtis, and C. T. Russell (1983), Wave structure in the Venus ionosphere downstream of the terminator, *Geophys. Res. Lett.*, *10*, 1116.

Brace, L. H., W. T. Kasprzak, H. A. Taylor, R. F. Theis, C. T. Russell, A. Barnes, J. D. Mihalov, and D. M. Hunten (1987), The ionotail of Venus: Its configuration and evidence for ion escape, *J. Geophys. Res.*, *92*, 15–26.

Brain, D. A., J. S. Halekas, L. M. Peticolas, R. P. Lin, J. G. Luhmann, D. L. Mitchell, G. T. Delory, S. W. Bougher, M. H. Acuña, and H. Rème (2006), On the origin of aurorae on Mars, *Geophys. Res. Lett.*, *33*, L01201, doi:10.1029/2005GL024782.

Cain, J. C., B. B. Ferguson, and D. Mozzoni (2003), An $n = 90$ internal potential function of the Martian crustal magnetic field, *J. Geophys. Res.*, *108*(E2), 5008, doi:10.1029/2000JE001487.

Dubinin, E., K. Sauer, and J. F. McKenzie (2006a), Nonlinear 1-D stationary flows in multi-ion plasmas—Sonic and critical loci—Solitary and oscillatory waves, *Ann. Geophys.*, *24*, 3041–3057.

Dubinin, E., et al. (2006b), Plasma morphology at Mars, ASPERA-3 observations, *Space Sci. Rev.*, *126*, 209.

Dubinin, E., et al. (2006c), Solar wind plasma protrusion into the Martian magnetosphere: ASPERA-3 observations, *Icarus*, *182*, 343.

Dubinin, E., et al. (2008a), Access of solar wind electrons into the Martian magnetosphere, *Ann. Geophys.*, in press.

Dubinin, E., et al. (2008b), Structure and dynamics of the solar wind/ionosphere interface on Mars: MEX-ASPERA-3 and MEX-MARSIS observations, *Geophys. Res. Lett.*, *35*, L11103, doi:10.1029/2008GL033730.

Dubinin, E., et al. (2008c), Suprathermal electron fluxes on the nightside of Mars: ASPERA-3 observations, *Planet. Space Sci.*, *56*, 846, doi:10.1016/j.pss.2007.12.010.

Dubinin, E., G. Chanteur, M. Fraenz, and J. Woch (2008d), Field-aligned currents and parallel electric field potential drops at Mars. Scaling from the Earth' aurora, *Planet. Space Sci.*, *56*, 868, doi:10.1016/j.pss.2007.12.019.

Duru, F., D. A. Gurnett, D. D. Morgan, R. Modolo, A. F. Nagy, and D. Najib (2008), Electron densities in the upper ionosphere of Mars from the excitation of electron plasma oscillations, *J. Geophys. Res.*, *113*, A07302, doi:10.1029/2008JA013073.

Fraenz, M., et al. (2006), Plasma intrusion above Mars crustal fields—Mars Express ASPERA-3 observations, *Icarus*, *182*, 406.

Frahm, R. A., et al. (2006a), Carbon dioxide photoelectron energy peaks at Mars, *Icarus*, *182*(2), 371–382, doi:10.1016/j.icarus.2006.01.014.

Frahm, R. A., et al. (2006b), Locations of atmospheric photoelectron energy peaks within the Mars environment, *Space Sci. Rev.*, *126*, 389.

Gurnett, D. A., et al. (2005), Radar soundings of the ionosphere of Mars, *Science*, *310*, doi:10.1126/scince.1121868.

Gurnett, D., et al. (2007), An overview of radar soundings of the Martian ionosphere from the Mars Express spacecraft, *Adv. Space Res.*, *310*, 1929, doi:10.1016/j.asr.2007.01.062.

Haerendel, G., et al. (1986), Dynamics of the AMPTE artificial comet, *Nature*, *320*, 720.

Hanson, W. B., and G. P. Mantas (1988), Viking electron temperature measurements: Evidence for a magnetic field in the Martian ionosphere, *J. Geophys. Res.*, *93*, 7538.

Hanson, W. B., S. S. Sanatani, and D. R. Zuccaro (1977), The Martian ionosphere as observed by the Viking retarding potential analyzers, *J. Geophys. Res.*, *82*, 4351.

Kliore, A. J. (1992), Radio occultation observations of the ionospheres of Mar and Venus, in *Venus and Mars: Atmospheres, Ionospheres, and Solar Wind Interactions, Geophys. Monogr. Ser.*, vol. 66, edited by J. G. Luhmann, M. Tatrallyay, and R. Pepin, pp. 265–276, AGU, Washington, D. C.

Leblanc, F., et al. (2008), Observations of aurorae by SPICAM ultraviolet spectrograph on board Mars Express: Simultaneous ASPERA-3 and MARSIS measurements, *J. Geophys. Res.*, *113*, A08311, doi:10.1029/2008JA013033.

Luhmann, J. G., and T. E. Cravens (1991), Magnetic fields in the ionosphere of Venus, *Space Sci. Rev.*, *55*, 201.

Luhmann, J. G., R. J. Warniers, C. T. Russell, J. R. Spreiter, and S. S. Stahara (1986), A gas dynamic magnetosheath field model for unsteady interplanetary fields: Application to the solar wind interaction with Venus, *J. Geophys. Res.*, *91*, 3001.

Lundin, R., et al. (2006), Plasma acceleration above Martian magnetic anomalies, *Science*, *311*(5763), 980, doi:10.1126/science.1122071.

Lundin, R., S. Barabash, M. Holmström, H. Nilsson, M. Yamauchi, M. Fraenz, and E. M. Dubinin (2008), A comet-like escape of ionospheric plasma from Mars, *Geophys. Res. Lett.*, *35*, L18203, doi:10.1029/2008GL034811.

Ma, Y., A. F. Nagy, I. V. Sokolov, and K. C. Hansen (2004), Three-dimensional, multispecies, high spatial resolution MHD studies of the solar wind interaction with Mars, *J. Geophys. Res.*, *109*, A07211, doi:10.1029/2003JA010367.

Mazelle, C., et al. (1989), Analysis of suprathermal electron properties at the magnetic pile-up boundary of comet P/Halley, *Geophys. Res. Lett.*, *16*, 1035.

Modolo, R., G. Chanteur, E. Dubinin, and A. Matthews (2006), Simulated solar wind plasma interaction with the Martian exosphere: Influence of the solar EUV flux on the bow shock and the magnetic pile-up boundary, *Ann. Geophys.*, *24*, 3403.

Morgan, D. D., D. A. Gurnett, D. L. Kirchner, J. L. Fox, E. Nielsen, and J. J. Plaut (2008), Variation of the Martian ionospheric electron density from Mars Express radar soundings, *J. Geophys. Res.*, *113*, A09303, doi:10.1029/2008JA013313.

Nagy, A. F., et al. (2004), The plasma environment of Mars, *Space Sci. Rev.*, *11*(1–2), 38.

Pätzold, M., et al. (2005), A sporadic third layer in the ionosphere of Mars, *Science*, *310*, 837.

Picardi, G., et al. (2004), MARSIS: Mars Advanced Radar for Subsurface and Ionosphere Sounding, in *Mars Express: A European mission to the Red Planet*, edited by A. Wilson, *Eur. Space Agency Spec. Publ.*, *ESA-SP 1240*, 5170.

Russell, C. T., J. G. Luhmann, and R. J. Strangeway (2006), The solar wind interaction with Venus through the eyes of the Pioneer Venus Orbiter, *Planet. Space Sci.*, *54*, 1482.

Safaeinili, A., W. Kofman, J. Mouginot, Y. Gim, A. Herique, A. B. Ivanov, J. J. Plaut, and G. Picardi (2007), Estimation of the total electron content of the Martian ionosphere using radar sounder surface echoes, *Geophys. Res. Lett.*, *34*, L23204, doi:10.1029/2007GL032154.

Sauer, K., and E. Dubinin (2000), The Martian 'obstacle' boundary, *Adv. Space Res.*, *26*(10), 1633.

Spreiter, J. R., A. L. Summers, and A. W. Rizzi (1970), Solar wind flow past nonmagnetic planets—Venus and Mars, *Planet. Space Sci.*, *18*, 1281.

Szego, K., et al. (2000), Physics of mass-loaded plasmas, *Space Sci. Rev.*, *94*, 623.

Valenzuela, A., et al. (1986), The AMPTE artificial comet experiments, *Nature*, *320*, 700.

Vennerstrom, S., N. Olsen, M. Purucker, M. H. Acua, and J. C. Cain (2003), The magnetic field in the pile-up region at Mars, and its variation with the solar wind, *Geophys. Res. Lett.*, *30*(7), 1369, doi:10.1029/2003GL016883.

————————

F. Akalin, F. Duru, D. A. Gurnett, and R. Modolo, Department of Physics and Astronomy, University of Iowa, Iowa City, IA 52242, USA. (ronan-modolo@uiowa.edu)

S. Barabash and R. Lundin, Swedish Institute of Space Physics, P.O. Box 812, SE-981 28 Kiruna, Sweden. (stas@irf.se; rickard@irf.se)

G. Chanteur, Centre d'Etude des Environnements Terrestres et Planétaires, IPSL, F-37191 Velizy, France.

E. Dubinin, M. Fraenz, and J. Woch, Max-Planck-Institute for Solar System Research, Max-Planck-Str. 2, D-37191 Katlenburg-Lindau, Germany. (dubinin@mps.mpg.de)

R. Frahm and J. D. Winningham, Southwest Research Institute, P.O. Drawer 28510, San Antonio, TX 78228-0510, USA.

G. Picardi, Infocom Department, "La Sapienza" University of Rome, I-00184 Rome, Italy.

J. J. Plaut, Jet Propulsion Laboratory, 4800 Oak Grove Drive, Pasadena, CA 91109, USA.